

# Complex- $k$ modes of plasmonic chain waveguides

M. Yan\*

Department of Applied Physics,  
School of Engineering Sciences,  
KTH - Royal Institute of Technology  
Isafjordsgatan 22, Kista 16440, Sweden

(Dated: February 13, 2019)

Nanoparticle chain waveguide based on negative-epsilon material is investigated through a finite-element-based mode solver which derives complex propagation constants ( $k$ ) of propagating modes. We first look into waveguiding behavior of chain waveguides made of non-dispersive negative-epsilon material. Such study singles out “waveguide dispersions”, which not only answers when indeed we need to consider such discrete waveguides rather than more traditional uniform waveguides, but also reveals modal properties over a broad spectrum for a certain geometry and permittivity setting, motivating search of new materials for desired guidance at unconventional wavelengths. We then examine chain waveguides made of realistic dispersive and lossy materials, from classic noble metal particles to doped silicon. Performance of more complicated geometries, such as hetero-plasmonic and chain-on-substrate systems, are also studied. In general, chain waveguides based on natural plasmonic materials are found to be quite lossy, with propagation length on the order of input light wavelength. Despite short propagation lengths, this work provides a more complete understanding of this class of waveguides which might be useful for their further developments towards practical information- and energy-transfer applications.

## I. INTRODUCTION

Optical waveguide formed by a chain of metal nanoparticles (*chain waveguide* in short) was proposed in [1] as an alternative to axially invariant plasmonic waveguides for shrinking footprint of photonic integrated circuits. Such a waveguide relies on coupled electromagnetic (EM) resonances in negative-epsilon particles to relay optical wave. The particles are usually in deep-subwavelength scale such that they can be treated as dipoles. That a chain of coupled dipoles can channel EM power without any radiation leakage contrary to stand-alone dipoles is in a sense an extreme case where radiation of a dipole is heavily affected by its environment. From waveguiding point of view, it can be argued that such propagation of EM wave in a periodic material system is fundamentally indifferent from those all-dielectric periodic waveguides presented in [2–4], some of which were referred to as coupled-resonator optical waveguides (CROWs). What make the waveguides under current investigation distinct are the “plasmonic” nature of the modes as well as the strong material dispersion, and thereby loss, usually associated with negative-epsilon materials.

Figure 1(a) illustrates a schematic picture of such waveguide. The metal nanoparticles are contained in a dielectric environment. Such a chain structure in its simple setting has been studied mostly through theoretical calculations [1, 5–10] and, in very few occasions, through experiments [11, 12]. Most studies so far focused on modes based on the fundamental dipolar resonance of metallic nanoparticles. Existing understanding of these fundamental modes based on previous work is

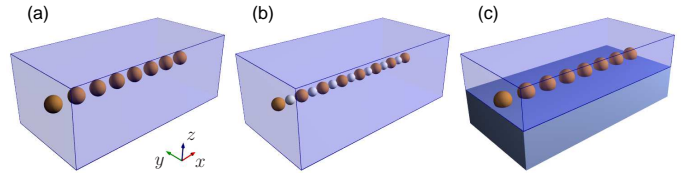


FIG. 1. Schematic diagrams of three types of chain waveguides. (a) Ideal chain waveguides based on negative-epsilon nanoparticles. Background medium (light blue region) can be a dielectric material or vacuum/air. (b) A chain waveguide consisting two types of particles (silver- and gold-colored). (c) A chain waveguide with dome-shaped particles sitting on some substrate.

summarized as follows. Unlike uniform waveguides like optical fibers, the resonant nature of chain waveguides determines that light propagation in such waveguides is relatively narrow-band, with transmission frequencies decided roughly by the resonant frequencies of individual nanoparticles. Depending on major polarization, there exist two types of low-order chain modes: transverse mode (T mode) with electric field majorly directed normal to waveguide axis ( $x$  in this work, Fig. 1) and longitudinal mode (L mode) with electric field majorly directed along waveguide axis. T mode appears in a degenerate pair since the waveguide is rotationally symmetric with respect to the waveguide axis. The L mode is unik for chain waveguides based on negative-epsilon materials; its polarization is seemingly incompatible with the transverse-EM (TEM) nature of light. Both T and L modes can be deep-subwavelength (yet it was not pointed out when such tight guidance can be obtained). Due to almost inevitable lossy nature of all negative-epsilon materials, guided modes in chain waveguides tend to have a large propagation loss. Precise calculation or demonstra-

\* miya@kth.se

tion of propagation loss, especially its wavelength dependence, was very scarce. In [1], it was found after geometrical optimization that propagation length for a silver chain waveguide in air/vacuum is as low as  $\sim 0.9 \mu\text{m}$  at near-ultraviolet (UV) wavelength. The limited propagation length with silver particles has somewhat discouraged further investigation of such waveguides. We think that there are aspects of such waveguides that are not fully examined. There exist more variations of chain waveguide setups. For example, instead of air or a homogeneous dielectric background, more complicated environment is possible — non-spherical particles sitting on a solid substrate can be a more realistic configuration (Fig. 1c). A recent work [13] demonstrated that a silver nanoparticle placed in between two gold nanoparticles can increase energy transfer between the two gold particles. A natural question arises whether a hetero-plasmonic chain waveguide, or one chain with two types of metal particles (Fig. 1b), can potentially have an increased propagation length fulfilling practical application needs. Also, besides noble metals for visible and near-infrared (NIR) plasmonics, doped semiconductors has become an emerging plasmonic material for applications at mid-infrared (MIR) frequencies [14–17]. There is lack of theoretical evaluation of such MIR chain waveguide.

To rigorously analyze a plasmonic chain waveguide is certainly not a trivial numerical task. Previously the dominant analysis methods include quasi-static dipole approximation with damping correction at optical frequency [5], and eigen-decomposition method in [6, 9, 10]. The dipole approximation method derives complex frequency as its eigenvalue. The wave number or propagation constant  $k$  of each mode is read from the mode patterns. The imaginary part of frequency denotes the lifetime of the oscillating mode. Such mode corresponds to a situation where a chain is uniformly excited by a plane-wave EM field, whereas in a waveguide problem one is more interested in finding a complex wave number with a given real frequency (as laser sources usually have). The imaginary part of  $k$  denotes spatial decay of a mode along the waveguide. The eigen-decomposition methods solves for scattering spectra against frequency and wave number, both in real values. The width of the bands in frequency is interpreted as the mode qualities. The iterative calculations of scattering spectra can however be a lengthy process. To the best of the author’s knowledge, there has been very few reports on direct solution of complex- $k$  modes in chain waveguides with real frequency as input. The only work doing such direct calculation is found in [7, 8], where a semi-analytical method was formulated using Mie theory with lowest-order approximation. All the approaches mentioned above by default only handle waveguide made of identical nanoparticles, and usually difficult if not impossible to include a substrate. The current work aims to use an empirical mode solver based on finite-element method (FEM) to study guidance properties of chain waveguides in a broader context. The numerical mode solver is implemented through

weak-form Galerken formulation, which calculates modes with complex wave vectors against a real frequency input in a periodic material system [18]. By deploying perfectly matched layers (PMLs)[19] around chain waveguide to emulate open-boundary condition and restricting wave vector (thereby also periodic boundary condition) along waveguide axis, one can find complex- $k$  propagating modes of chain waveguides. As the method is fully numerical, it can handle any particle geometry or material composition (including multiple dissimilar particles) in a unit cell and even CROW waveguides or more recently subwavelength gratings [20]. High-order modes based on multipolar particle resonances can also be calculated; however they are not of focus in the current study. Throughout this work, we deploy time-harmonic convention of  $\exp(i\omega t)$ . A forward-propagating wave along  $+x$  then has spatial dependence  $\exp(-ikx)$ , where the complex wave number is expressed as  $k = k_r + k_i i$ .  $k_r$  must be positive;  $k_i$  is negative for decaying field, and positive for amplifying field.

Since noble metals have complex, wavelength-dependent permittivity values, chain waveguides made from them can be rather complicated to comprehend. Following Introduction, in Section II, the investigation starts with waveguides made of material with a real, wavelength-independent negative-epsilon value. Such analysis with non-dispersive material was exercised quite often in dielectric photonic-crystal studies for capturing key modal propagation characteristics. In such a simplified setting, one clearly identifies the “waveguide dispersion” (effect of geometry on modal dispersion, as commonly referred to in fiber optics community), instead of seeing mixed effect contributed also by variation in permittivity. In the meantime, modal properties at different frequencies can be related to distinct materials possessing such permittivity values, which motivates us to look for new negative-epsilon materials beyond the traditional noble metals. The analysis will show how modal behavior changes after material absorption loss is introduced. Section III then looks into waveguides made of realistic dispersive materials, including silver and gold for visible-light guidance. The performance of hetero-plasmonic waveguide will, for the first time, be presented. The effect of background medium including presence of a substrate will also be examined. Last, we show the prospect (or limitation) of using heavily-doped silicon for potentially guiding light at mid-infrared (MIR) wavelengths. Conclusion follows in the end.

## II. NON-DISPERSIVE METAL WAVEGUIDE

### A. Lossless chain

As mentioned in [2], for a certain 1D periodic waveguide, there is a general upper frequency limit for guided mode. The limit is set by the crossing point between light line in background medium (i.e.  $\omega = kc/n_b$ ) and

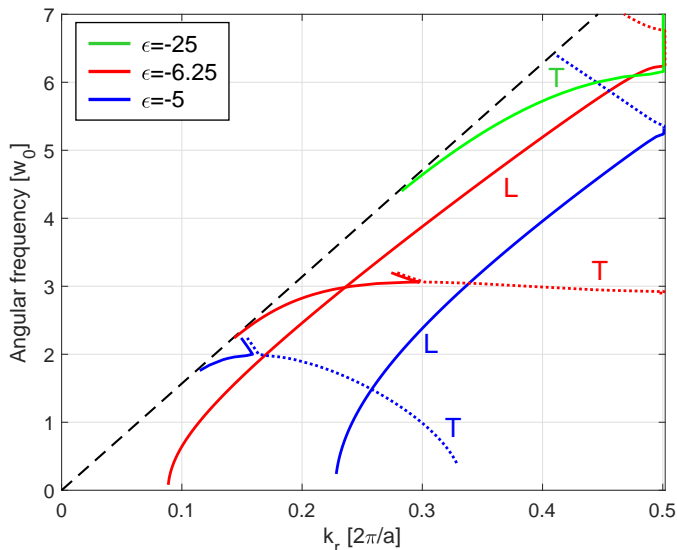


FIG. 2. Modal dispersion curves of chain waveguides with non-dispersive particle permittivity. Longitudinal (L) and transverse (T) modes are duly labeled for each dispersion curve. Geometry is fixed at  $a = 80$  nm and  $d = 60$  nm.  $\epsilon_b = 2.25$ . Three particle permittivity values are studied, as shown in different colors. Dotted lines correspond to portions of dispersion curves with negative slopes. Note: dotted lines for  $\epsilon_m = -5, -6.25$  are shifted by  $+0.005 \times 2\pi/a$  in  $k_r$  to show the degenerate part. Dashed line is light line of the background medium.

the first Brillouin zone boundary ( $k_{bz} = \pi/a$ ).  $k$  is wave number;  $c$  is speed of light; and  $n_b$  is refractive index of background medium. Correspondingly, guided wavelength for a certain chain waveguide has to be

$$\lambda > 2n_b a. \quad (1)$$

The above equation can be used for determining an appropriate period  $a$ , as the guiding wavelength  $\lambda$  for a chain waveguide is associated with the particle-plasmon resonance. Take silver as an example. As a rough estimation, silver has plasma frequency  $w_p = 1.39 \times 10^{16}$  rad/s according to Drude-model fitting [21], which leads to their particle resonance approximately at  $w_p/\sqrt{3}$  in frequency or 235 nm in wavelength. For achieving light guidance at such wavelength using chain waveguides, one shall use a period of 117 nm or below in the case of vacuum background medium. In the following study, the reference structure has period  $a = 80$  nm with a background medium of refractive index  $n_b = \sqrt{\epsilon_b} = 1.5$  (which can be associated with many glass materials). The guided mode is expected above free-space wavelength ( $\lambda_0$ ) of 240 nm. Particle size as characterized by diameter  $d$  in our primary focus is chosen as 60 nm. The above analysis, as will be shown in Section III, is only a rough estimation; guided chain mode can be dispersive, and exists for silver-chain case at up to  $\lambda_0 = 550$  nm.

Before we look into realistic plasmonic metals, we study mode properties of chain waveguides made of fic-

titious non-dispersive “metal” particles. Three distinct permittivity values ( $\epsilon_m = -5, -6.25, \text{ and } -25$ ) are considered, with background medium  $\epsilon_b = 2.25$ . The calculated bands for modes identified (also called modal dispersion curves) are shown in Fig. 2. Note that in the case of non-dispersion material, scaling law is fulfilled. That is, both frequency and wavevector can be normalized against some length metric (most often period of the structure). However, since in this work we will also study dispersive chain waveguide, for ease of comparison we choose to normalize angular frequency against  $\omega_0 = 10^{15}$  rad/s. Wavevector is normalized against  $2\pi/a$ , as conventionally done in photonic-crystal analyses. Wavevector is in general a complex number, which is even true for all-real permittivity values used. Modes with frequency falling in photonic band gaps carry such a complex  $k$  value, with its imaginary part denoting its degree of attenuation. Consequently, mode searching was in general carried out in complex wavevector plane for a given frequency. Only guided modes under light line of the background medium are searched. As a common practice for periodic systems, Fig. 2 only shows bands in the first Brillouin zone (BZ), with positive  $k_r$ .

As revealed in Fig. 2, the chain waveguide in general possesses both T and L modes over the examined frequency range. The dispersions of modes can be quite peculiar as compared to conventional all-dielectric waveguides. The dispersion curves of T modes are seemingly stemming out of the light line of background medium at small  $k_r$  values. This feature is shared by modes in dielectric waveguides, and is fundamentally due to the fact that the T mode and the mode corresponding to the light line have the same TEM symmetry. Different from bands in dielectric waveguides, here in the plasmonic case, the T-mode dispersion curves can reach a maximum in frequency and thereafter exhibit a negative slope (represented by dotted-line sections). Negative-slope dispersion curves were previously considered for realizing light propagation with negative group velocity (-GV), and the plateau point in a dispersion curve for achieving “stopped” light with zero GV (0GV). However, as will be shown in Fig. 4, dispersion close to 0GV point or with small GV in general is highly susceptible to material loss. Note that at the 0GV position, T modes from +GV and -GV sections converge and become a degenerate pair; the pair branches out towards high frequency with a steep slope, at the same time their  $k$  values turning into a complex-conjugate pair (Fig. 4). This is a signature that the modes from both +GV and -GV sides enter into a photonic band gap regime, as was also noticed in [7]. In contrast, for non-dispersive dielectric photonic structures, extremities of a band occurs at either center or edge of its BZ. The L mode in Fig. 2 has a more intriguing dispersion profile. First, L mode has no coupling with light line of the background medium. This is fundamentally due to the unik polarization nature of the mode. Second, if it does not reside in the radiation cone of the background medium (which we did not look

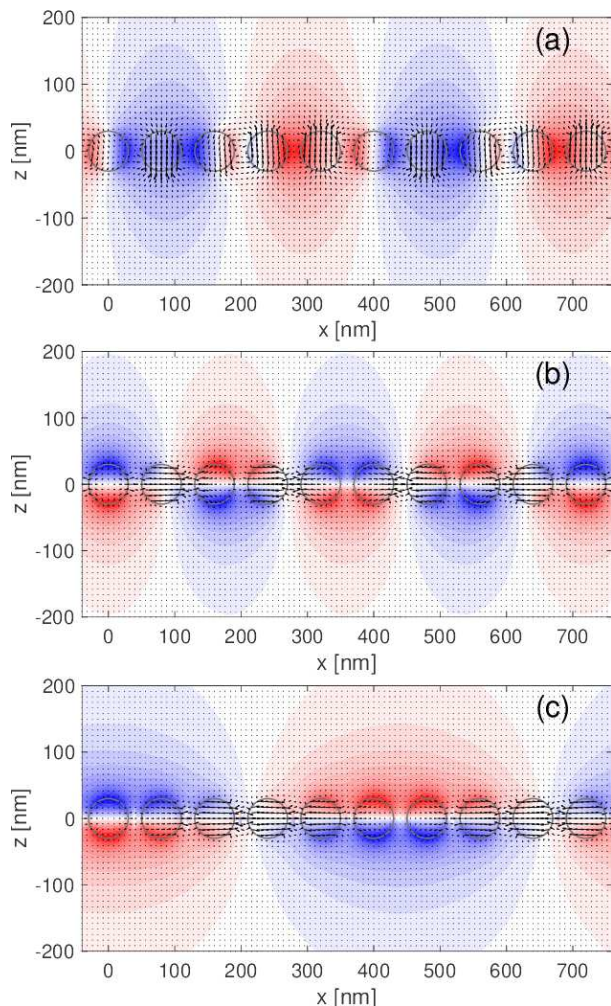


FIG. 3. Fields of lossless chain waveguides.  $a = 80$  nm,  $d = 60$  nm,  $\epsilon_m = -6.25$ , and  $\epsilon_b = 2.25$ . (a,b) T and L modes at  $\omega = 2.8\omega_0$ . (c) L mode at  $\omega = 0.3\omega_0$ . The arrows denote displacement field, while the colormaps denote magnetic field component along  $y$ , i.e.  $H_y$ . Red and blue colors correspond to positive and negative field amplitudes, respectively.

into), the L mode persists over a very broad frequency range, even when frequency approaches zero. This suggests such a nanostructured chain waveguide (especially with small particle permittivity value) can potentially guide light with a very long wavelength. In addition, the guided mode can have a very large effective mode index  $n_{\text{eff}} = k_r/k_0$ ; therefore deep-subwavelength guidance can be ensured.

When the particle permittivity value increases negatively, in general, the dispersion curves shift to higher frequencies. This can be explained by the fact that the particles become more and more metallic at large negative permittivity values; thereby EM field is squeezed more out of the particles. Resonance is sustained by effectively smaller and low-index space surrounding the particles, hence the higher frequencies observed.

EM field patterns of three representative modes are

presented in Fig. 3. Only cases for  $\epsilon_m = -6.25$  are plotted. For ease of interpretation, the fields are constructed over multiple cells based on Floquet theorem to reveal full-wavelength evolutions. Panels (a) and (b) show the T and L modes at  $\omega = 2.8\omega_0$ , respectively. The frequency corresponds to  $\lambda_0 = 673$  nm. The plots visualize clearly orientation and coupling of particle dipoles, as well as wavelength of the guided wave (thereof  $n_{\text{eff}}$  and mode confinement). For the T mode in Fig. 3(a), it has a major magnetic field directed along  $y$  direction, i.e.  $H_y$  component (as shown by the colormap in the figure). Whereas, the L mode in Fig. 3(b) has its magnetic field curling around the waveguide axis. Comparatively, the L mode is somewhat similar to the so-called transverse-magnetic mode in cylindrical optical fibers. Figure 3(c) shows an L mode at relatively a low frequency of  $0.3\omega_0$ , corresponding to  $\lambda_0 = 6.28$   $\mu\text{m}$ . Deep-subwavelength guidance at the MIR frequency is then achieved. We will discuss the possibility of achieving such guidance using e.g. doped silicon in Section III.

The L mode is heavily affected by the particle spacing. A study with a period of 100 nm (particle permittivity remains at -6.25) shows that the L-mode band is markedly blue-shifted, by  $\sim 21\%$  at  $k_r = 0.3[2\pi/a]$  (where  $a = 100$  nm), whereas the T-mode band is almost unchanged (increase in frequency less than 2% at the same wave number). Smaller particle tends to increase frequencies of the bands. This is confirmed with a calculation of dispersion curves for a chain waveguide with  $a = 80$  nm and  $d = 40$  nm, again with the same particle permittivity (results not shown).

## B. Lossy chain

In the above sub-section, only lossless chain waveguides were studied. As a matter of fact, material losses associated with negative-epsilon materials are usually quite significant. Here we look into the effect of adding an imaginary part to the particle permittivity. Still, the considered particles will have non-dispersive permittivity. Similar to the previous sub-section, the focus is on chain waveguide with  $a = 80$  nm,  $d = 60$  nm, and  $\epsilon_b = 2.25$ . A frequency-independent loss tangent of 0.01 is added to the material, i.e.  $\epsilon_m = \epsilon_r + \epsilon_i i = -6.25 - 0.0625i$ .  $\epsilon_i$  is negative for lossy material as a result of the time-harmonic convention used.

In Fig. 4(a), dispersion curves obtained for the lossless and lossy chain waveguides are compared. As mentioned previously, even with all-real permittivity values, the mode solver obtains modes with complex  $k$ , more specifically for modes falling in photonic band gaps. When material loss is introduced, modes at all frequencies carry complex  $k$  values. The imaginary part of  $k$  ( $k_i$ ) is plotted in Fig. 4(b). For a reason to be clarified in the following paragraph, our trace of dispersion stops when  $k_i$  reaches  $\sim 0.1$  or beyond. There are two observations worth commenting for Fig. 4. First (already pointed out in last



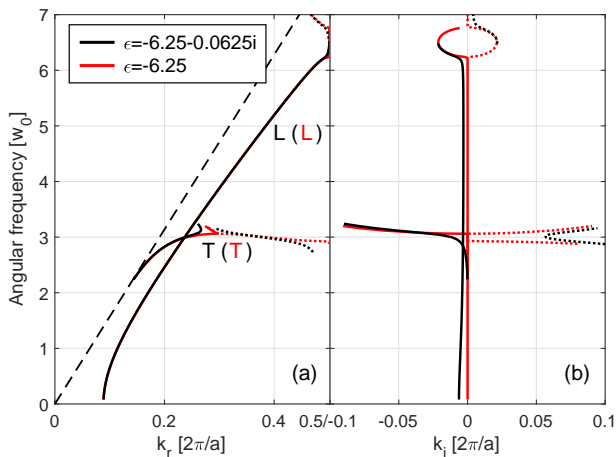


FIG. 4. Effect of material loss on modal dispersion curves of chain waveguides.  $a = 80$  nm,  $d = 60$  nm, and  $\epsilon_b = 2.25$ . Metal particle has  $\epsilon_r = -6.25$  with or without an imaginary part of  $\epsilon_i = 0.01\epsilon_r$ . Bands corresponding to T and L modes are labeled.

sub-section), when loss is added, dispersion curve close to an originally 0GV point is highly affected. For the T mode, there are two 0GV points, one at the plateau point of its dispersion curve and the other at the BZ boundary. With material loss, the slopes of the dispersion curves at those positions tend to increase rather than to approach zero. At the same time,  $k_i$  increases sharply. A direct consequence is that T mode with -GV (dashed black line) becomes highly lossy. The more useful T-mode dispersion curve (remaining +GV section, solid black curve) bends back in  $k_r$  before reaching the plateau point, towards the originally degenerate mode-pair branch. The bending starts sooner as material loss increases. This observation suggests that small-GV modes are highly vulnerable to material losses; 0GV is simply not possible. Similar finding on effect of material loss on GV was also described in our previous investigation regarding a light absorbing structure [22]. The second observation is that dispersion-curve sections with negative slopes (dotted lines in Fig. 4) are associated with modes with amplifying amplitudes as they propagate in  $+x$  direction, which is manifested by their positive  $k_i$  values. In the current study, such amplifying mode propagation applies to both the upper section of L band and the -GV section of the T band. The effects and consequences of such amplifying modes will be investigated in a separate study.

Propagation length  $L_p$  of a mode (distance for mode intensity decreasing to its  $1/e$ ) is calculated from imaginary part of wave vector as  $L_p = -1/(2k_i)$ , i.e.  $L_p$  inversely proportional to  $k_i$ . When amplifying modes are concerned,  $k_i$  is positive and the distance in absolute value corresponds to a mode's intensity increased to its  $e$  times; we can refer to this length particularly as amplification length. For reference, a mode with  $k_i = -0.1 [2\pi/a]$  with  $a = 80$  nm has a propagation length of 64 nm. This is already smaller than the waveguide's period, ren-

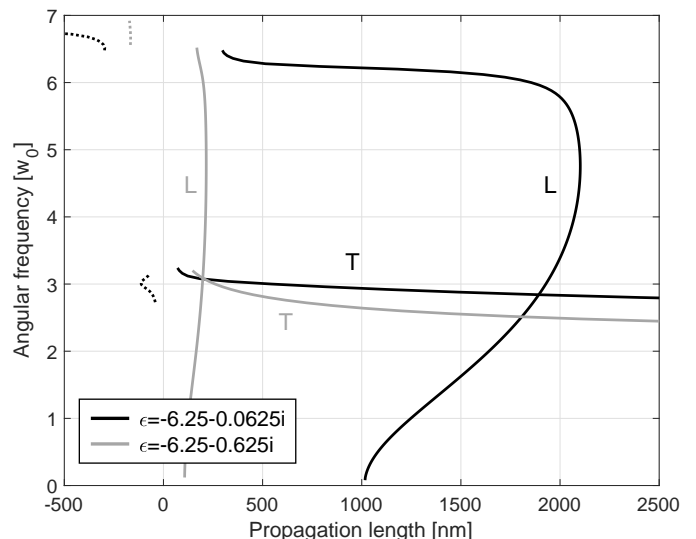


FIG. 5. Propagation length of chain-waveguide modes with particle material at two different loss levels.  $a = 80$  nm,  $d = 60$  nm,  $\epsilon_b = 2.25$ . Metal particles have real permittivity  $\epsilon_r = -6.25$ , and a loss tangent of 0.1 or 0.01.

dering therefore such a waveguide almost useless at the frequency considered. We plot in Fig. 5 the propagation lengths for modes of the waveguide at two loss tangents (0.1 and 0.01). The plot can be examined together with Fig. 4. Amplification lengths are plotted in negative values. The T mode is found to be extremely sensitive to frequency. Its  $L_p$  can be relatively long (beyond 1000 nm) in a short frequency range; however the long- $L_p$  modes are quite close to the light line and therefore their modal confinements are compromised. The L mode can sustain a consistent level of propagation length over a large frequency range. Comparing the propagation lengths at two loss levels, one finds the propagation length is roughly inversely scaled to the imaginary part of metal permittivity. Subwavelength mode confinement of L modes can be guaranteed as its dispersion curve can stay quite far below the light line, especially when small negative permittivity is used for particles (see Fig. 2). This observation hints that it would be interesting to look for new materials with small negative permittivities for subwavelength light guiding at especially low frequencies.

### III. REAL-METAL WAVEGUIDE

In this section we first consider two classic noble metals, i.e. gold (for its chemical stability) and silver (for its lower loss at visible and NIR). The data for silver and gold are taken from [21]; their analytical Drude models are not used since the fittings are more relying on long-wavelength data and having large discrepancy at near-UV wavelength regions. Experimentally measured permittivity data [21] show gold has a much higher loss than silver at UV and visible spectrum. For example,

at  $\lambda_0 = 550$  nm silver has  $\epsilon_{\text{Ag}} = -13 - 0.43i$  and gold has  $\epsilon_{\text{Au}} = -6 - 2.1i$ , i.e 10 times difference in terms of loss tangent. Later in the section, we will discuss performance of chain waveguides at MIR frequencies, by using heavily-doped silicon. Such MIR plasmonic material has its permittivity characterized by a Drude model, as to be presented therein.

### A. Silver or gold chain

In Fig. 6 we lump together dispersion curves calculated for a silver chain waveguide (blue curves) and those for a gold chain waveguide (red curves), both with  $a = 80$  nm,  $d = 60$  nm, and  $\epsilon_b = 2.25$ . In general the dispersion curves for the silver chain waveguide appear at higher frequencies (3.4–4.8  $\omega_0$ , or 550–400 nm in free-space wavelength, respectively), while the modes for gold chain waveguides appear at 3–3.6  $\omega_0$  (630–520 nm in free-space wavelength, respectively). This is in agreement with the fact that the plasma frequency of silver is higher than that of gold. As suggested by permittivity values, the silver chain waveguide suffers less propagation loss compared to the gold counterpart. For the gold waveguide, the material is so lossy that its T-mode dispersion curve tends to fold back as soon as it stems out of the light line; as a result, the T-mode dispersion curve nearly laps over the background light line. The mode is therefore quite delocalized. The L mode has better confinement but it carries a  $k_i$  around 0.1, hence difficult to channel light across a distance larger than a period. The silver waveguide is comparatively less lossy. At  $\omega = 3.91\omega_0$  and below, the T mode has  $L_p > 1000$  nm, with diverging  $L_p$  as frequency decreases (to  $L_p = 54\mu\text{m}$  at  $\omega = 3.4\omega_0$ ). The L mode has  $L_p > 1000$  nm when  $\omega < 4.17\omega_0$  (until

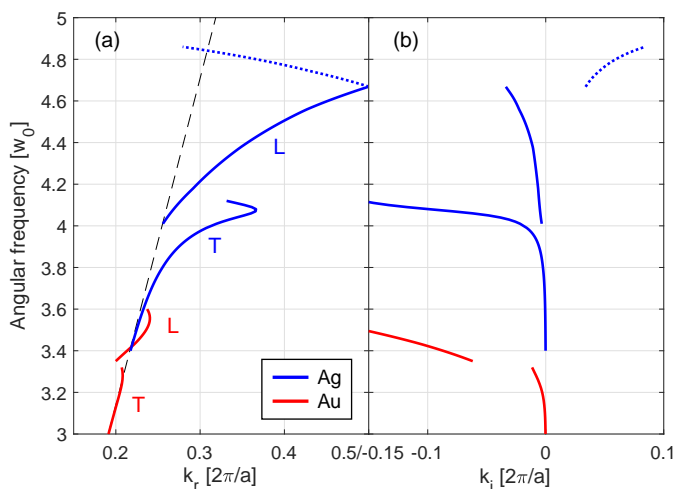


FIG. 6. Dispersion curves of modes guided in a silver (blue curves) or a gold (red curves) chain.  $a = 80$  nm,  $d = 60$  nm, and  $\epsilon_b = 2.25$ . Both L and T modes are shown. (a) Real part of  $k$ ; (b) imaginary part of  $k$ .

$4\omega_0$  where  $L_p = 1890$  nm). The results suggest that silver chain, especially its T-mode, can be potentially used for channeling light at limited visible wavelength ranges. That said, it should be pointed out that not all guidance is subwavelength; modes with long  $L_p$  can be due to that they stay close to the light line, and therefore with their fields extended in the background medium. One has to make a careful comparison to other types of waveguides, plasmonic or not, in terms of some figure of merit based on loss and mode confinement. The L mode tends to have deep-subwavelength guidance. However, it has to be used with extreme care, since it only achieves larger than 1000 nm propagation in a less than 20 nm wavelength window, which can be further subject to experimental imperfections.

### B. Hetero-plasmonic chain

In Fig. 1(c), a heterogeneous chain waveguide is illustrated, where two types of metal spheres are interleaved. Such design was motivated by [13]. It was proposed in [13] that by inserting a silver nanoparticle in between two gold nanoparticles one can facilitate more efficient energy transfer between two gold particles. The argument was tested with plasmonic trimer structures, which was realized by a delicate DNA-based self-assembly procedure. The loss reduction in energy transfer was argued through reduced bandwidth of observed dark-field scattering spectrum. Energy transfer across a longer chain beyond the trimer structure was not discussed. Here we extend the idea to a hetero-plasmonic chain waveguide, and numerically check its modal properties including propagation length. It is worth noting that, in a *finite* Au-Ag-Au trimer structure, it was the energy transfer process between two *gold particles* that was examined and was found to be more efficient compared to two directly coupled gold particles; in an *infinite* hetero-plasmonic waveguide, energy transfer can happen through hopping between *silver particles*, which has also to be considered.

The hetero-plasmonic chain waveguide to be studied comprises of simultaneously silver and gold nanoparticles. Our FEM analysis uses a supercell with a period of 80 nm, including a gold particle of diameter 40 nm and a silver particle of diameter 30 nm (thereof a gap size of 5 nm).  $\epsilon_b = 2.25$ . The geometrical parameters as well as the background permittivity are very close to those studied in [13], where gold-to-gold distance is 78 nm and background was assumed to have  $\epsilon_b = 2.15$ . It turns out that the hetero-plasmonic waveguide under study is a very lossy waveguide — key modal features are killed by the presence of heavy material losses. In order to better explain the guidance mechanism, we first calculated its dispersion curves with imaginary part of gold and silver permittivity values reduced by a factor of ten [23]. The resulted dispersion curves for the guided modes are shown in Fig. 7(a) by the black curves. In order to know

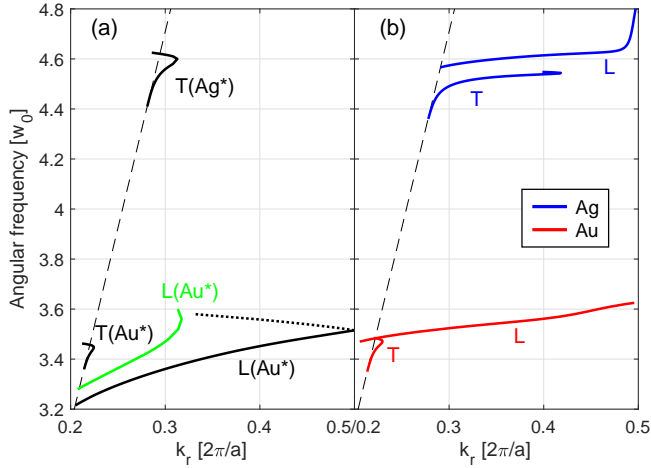


FIG. 7. (a) Modal dispersion curves of a hetero-plasmonic chain waveguide.  $a = 80$  nm,  $d_{\text{Au}} = 40$  nm,  $d_{\text{Ag}} = 30$  nm, and  $\epsilon_b = 2.25$ . The black curves are calculated with imaginary part of gold and silver permittivity values reduced by a factor of ten. The green curve is the only L mode remaining when the metals' losses take their realistic values. (b) Modal dispersion curves of two chain waveguides. One is gold chain waveguide with  $a = 80$  nm,  $d = 40$  nm, and  $\epsilon_b = 2.25$  (red curves). The other is silver chain waveguide with  $a = 80$  nm,  $d = 30$  nm, and  $\epsilon_b = 2.25$  (blue curves). In both cases, metals have their imaginary permittivities reduced by a factor of ten. Dashed line is light line of background medium.

the nature of the modes we plot three representative modal fields, one for each dispersion curve, in Fig. 8. Examination of the mode fields reveals that the bands correspond to T and L modes dominantly contributed by resonance in gold particles (around  $3.4\omega_0$ ) and a T mode dominantly contributed by resonance in silver particles (around  $4.5\omega_0$ ). The fact that one type of particles is clearly in resonance (dipolar) while the other is not (acting somewhat like spacers) suggests that a hetero-plasmonic waveguide can rather be treated as two superposed “homo-plasmonic” chain waveguides. Each homo-plasmonic chain contain a single-type particles with relatively large inter-particle spacings.

In Fig. 7(b) we present the dispersion curves of gold/silver homo-plasmonic chain waveguides, both with period  $a = 80$  nm but particle diameter  $d = 40$  nm for gold case and  $d = 30$  nm for silver case. The gold chain waveguide has T and L bands around  $3.5\omega_0$ , corresponding well to the lower set of modes in Fig. 7(a). The silver chain waveguide has T and L bands around  $4.5\omega_0$  with the T mode corresponding well to the upper T band in Fig. 7(a). The L mode in silver chain waveguide finds no counterpart in the hetero-plasmonic case due to two reasons. First, at that frequency gold is simply too lossy; and second, the electric field of the expected L mode has to majorly pass through the gold particles. If one examines the curves for modes' propagation lengths (not shown), one can conclude that: by superimposing two homo-plasmonic chains into one hetero-plasmonic chain

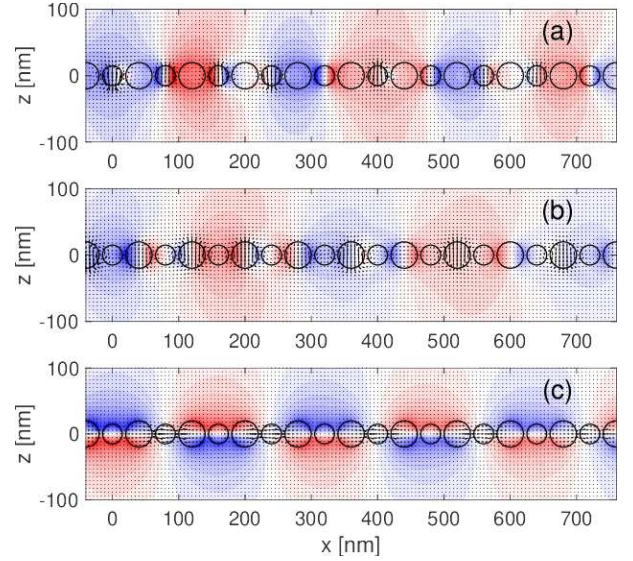


FIG. 8. Representative mode fields of the hetero-plasmonic chain waveguide.  $a = 80$  nm,  $d_{\text{Au}} = 40$  nm,  $d_{\text{Ag}} = 30$  nm,  $\epsilon_b = -6.25$ . (a) T mode at  $\omega = 4.55\omega_0$ ; (b) T mode at  $\omega = 3.44\omega_0$ ; (c) L mode at  $\omega = 3.30\omega_0$ . The arrows denote displacement field, while the colormaps denote magnetic field component along  $y$ , i.e.  $H_y$ . Red and blue colors correspond to positive and negative field amplitudes, respectively. Imaginary parts of gold and silver permittivities are reduced by a factor of ten. Fields attenuate as a result of material absorption.

waveguide, the chain modes supported by silver particles suffer higher losses with the L mode disappearing completely; for the gold chain, its T mode becomes a bit lossier, but the L mode can propagate much longer. More specifically, the L mode of gold chain (Fig. 7b has propagation length ranging from tens of nanometers at its high-frequency end to 400 nm at its low-frequency end ( $3.470\omega_0$ ); the corresponding L mode in hetero-plasmonic chain (Fig. 7a, solid black line) has 140 nm at its high-frequency end and  $\sim 1900$  nm at the low-frequency end ( $3.215\omega_0$ ). We refer to the gold-dominated L mode in the hetero-plasmonic chain waveguide as L(Au\*) mode, and similar to others.

In [13], the resonant modes were probed through optical scattering spectra. If translated onto our Fig. 7(a), their observed modes are within the light cone, close to the  $k_r = 0$  axis if it was nearly normal incidence). Their experiment recorded the dominant resonance peak [corresponding to L(Au\*) mode] shifted “from 549 nm for the AuNP (gold nanoparticle) homodimer to 586 nm for the heterotrimer structure”. These two peaks are respectively  $3.456\omega_0$  and  $3.214\omega_0$  in frequency, which project quite well to the curves that we have simulated. In [13], the increase in mode quality was explained through concepts such as “plasmonic hotspots” and “quasi-resonant virtual state” of silver particle, however we argue that the increase of mode quality is merely due to the fact that inclusion of silver particles decreases the L(Au\*) mode

to a lower frequency where gold material has smaller absorption loss. Losses of silver material does not adversely affect mode quality of the L mode significantly, since within that frequency gold has a loss tangent in average ten times as large as that of silver.

When metals take their 100% material losses, there is only one gold-dominated L mode remaining, as shown by the green curve in Fig. 7(a). Unfortunately its propagation length is found to be less than 100nm.

The phenomenon of enhanced energy transfer is geometry-dependent. We looked into a hetero-plasmonic waveguide with gold and silver particles with identical diameter  $d = 60$  nm and a gap size of 20 nm. The gold-dominated L mode disappeared, possibly due to too large separation between the gold particles.

Philosophically, it can be argued that that a hetero-plasmonic chain waveguide is an improved gold-chain waveguide or a deteriorated silver-chain waveguide.

We observed, through FEM analyses, that one can insert dielectric (e.g. silicon or  $\text{TiO}_2$ ) particles in a plasmonic chain to create hybrid plasmonic-dielectric chain waveguide. Whether such configuration has obvious advantage over hetero- or homo-plasmonic chain waveguide is worth further investigation.

### C. Background medium and substrate

The initial investigations on plasmonic chain waveguide used air/vacuum as the background medium [1, 5]. We calculated the dispersion curves of T and L modes of a silver-in-air chain waveguide with  $a = 80$  nm and  $d = 60$  nm (not shown). Compared to the corresponding curves for the silver-in-glass chain waveguide (Fig. 6), both bands experience a blue-shift in frequency when air is used. The respective shifts are roughly 26% for the T mode and 18% for the L mode, such that two bands are crossing each other in the air-background case. Direct comparison of propagation losses is not simple, as in two cases both modes are dispersive as well as that for each mode propagation loss is highly dependent on frequency. In general, use of air background does not markedly increase the propagation length of T mode; it actually shortens the propagation length of L mode as a result of more flattened dispersion curve of the mode. The L-mode band becomes more flat as a result of effectively shortened gap size between the particles — the chain mode is therefore made of more localized gap plasmons with less coupling among themselves.

Actual nanofabrication of chain waveguides can lead to a background that is more complex than a homogeneous medium. A more realistic version is a chain made of nanoparticles exposed in air but sitting on top of a dielectric substrate. Previously, the author and his colleagues have reported experimental demonstration of arrayed gold nanoparticles [24–26] on a dielectric substrate. The gold nanoparticles can have perfectly spherical shape, except with flattened bottom, similar

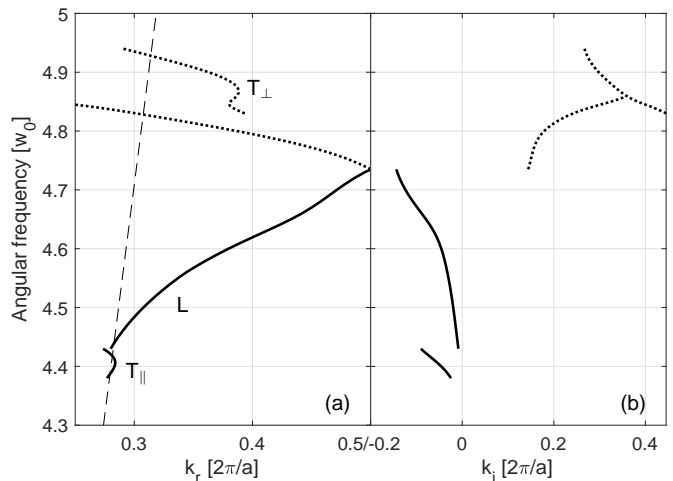


FIG. 9. Dispersion curves for modes guided by a dome-shaped silver-particle chain waveguide on a dielectric substrate.  $a = 80$  nm,  $d = 60$  nm. The particles' spherical center is located from substrate by a distance of  $d/4$ . (a) Dispersion; (b)  $k_i$ . Dashed line is the light line of the substrate material.

to droplets on a surface. The structure was achieved through light-induced rapid thermal annealing of lithographically patterned rectangular metal patches. The dome shapes are formed as a result of surface tension when they are melted. A chain waveguide made of such metal particles are schematically shown in Fig. 1(c). We choose silver for our following case study. It is believed that the above-mentioned thermal annealing technique can be applied equally well for silver. The chain waveguide we are to study has the following parameters:  $a = 80$  nm,  $d = 60$  nm, with a quarter of the sphere height truncated in the bottom. The substrate has  $\epsilon_s = 2.25$ . Rest of the background is air/vacuum.

The dispersion curves of modes identified as well as their  $k_i$  magnitude of the chain waveguide are plotted in Fig. 9. It is known that when a substrate is included, or when the particles depart from spherical symmetry, the degeneracy of the T-mode pair will be lifted. In other words, two T-mode dispersion curves will appear, one with major electric-field component directed perpendicular to the substrate ( $T_\perp$  mode) and the other with its major polarization parallel to the substrate while perpendicular to waveguide axis ( $T_\parallel$  mode). The two T-mode dispersion curves are depicted in Fig. 9(a).  $T_\parallel$  appears at frequency around  $4.4\omega_0$ , lower than that of the  $T_\perp$  mode (around frequency  $4.9\omega_0$ ). The  $T_\parallel$  mode has  $L_p < 250$  nm, which is due to the mode is closely coupled to radiation mode in the substrate material. The  $T_\perp$  mode carries a negative GV in general; its  $k_i$  has a quite large magnitude in average. The L mode exists in a relatively large frequency range with  $L_p < 800$  nm. Therefore, the propagation lengths obtained are in general not encouraging for information transfer purposes. However, such chain-on-substrate system can be an attractive platform for other nanophotonic uses. Especially, the L mode



exhibits strong gap-plasmon resonances; the enhanced electric field can be exploited for sensing and nonlinear-optics applications.

We mention that the waveguide geometry has not been optimized. It should be possible to tailor the particle shapes as well as to add more substrate layers to further increase propagation lengths of the modes.

#### D. MIR chain waveguide

MIR photonics is an emerging research topic which is critical for sensing, environment monitoring, biological imaging, etc. Doped semiconductors can become metallic at long EM wavelengths. Doped silicon, for example, can be interesting for integrated MIR photonics, where the fabrication process can be easily inherited from established CMOS technology. Drude model can be used for describing permittivity of doped silicon, as  $\epsilon(\omega) = \epsilon_\infty - \frac{\omega_p^2}{\omega^2 + i\frac{\omega}{\tau}}$ , where  $\epsilon_\infty$  is permittivity at high-frequency limit,  $\omega_p$  is plasma frequency, and  $\tau$  is collision time of free carriers. Plasma frequency is calculated as  $\omega_p^2 = \frac{Ne^2}{m^*\epsilon_0}$  with  $N$  doping concentration,  $e$  elementary charge,  $m^*$  effective mass of free carrier, and  $\epsilon_0$  vacuum permittivity. Following the numerical values adopted in [14], we choose  $n$ -doped silicon with  $\epsilon_\infty = 11.7$  and  $m^* = 0.272m_0$  ( $m_0$  is electron mass). Doping concentration chosen for the following case study is at  $N = 2 \times 10^{20} \text{ cm}^{-3}$ . Electron collision time can be calculated from measured carrier mobility as  $\mu = e\tau/m^*$ .  $\mu$  in [14] was stated as  $\mu = 50 \text{ cm}^2/(\text{V} \cdot \text{s})$  at the mentioned doping concentration, which led to  $\tau = 7.73 \text{ fs}$ . We find that with this collision time, Si permittivity has an imaginary part comparable to its real part, which is too lossy for making a waveguide. It was reported in [27] that electrons' mobility can increase significantly at lower temperature. At a doping concentration of  $1.3 \times 10^{17} \text{ cm}^{-3}$ ,  $\mu$  increases from  $\sim 500 \text{ cm}^2/(\text{V} \cdot \text{s})$  at room temperature to over  $4000 \text{ cm}^2/(\text{V} \cdot \text{s})$  at 50 K. Although there were no explicit experimental data for higher doping concentration scenario, here for a theoretical exploration, we assume a certain low temperature can increase  $\mu$  by a factor of eight for the considered doping concentration. Collision time increases correspondingly to  $\tau = 387 \text{ ps}$ . The overall objective of the setting, as inspired by Fig. 2, is to obtain a relatively small (less than 10) negative permittivity at MIR frequency such that deep-subwavelength MIR guidance can be realized using a chain waveguide made of such doped semiconductor materials. This idea can be extended naturally to chain waveguide design at even longer wavelengths.

By using the standard geometry in this work, i.e.  $a = 80 \text{ nm}$  and  $d = 60 \text{ nm}$ , together with the above-mentioned particle material setting, we find an L mode appearing around frequency  $0.4\omega_0$ , as shown by Fig. 10a. Inset in Fig. 10 gives the real and imaginary parts of silicon's permittivity at the relevant wavelength range. The

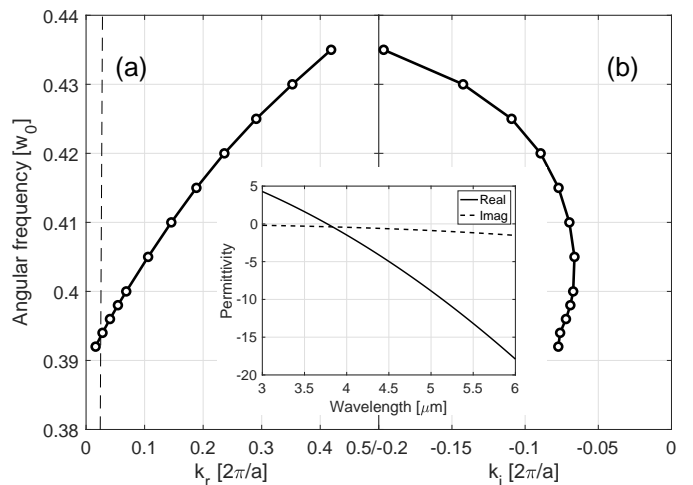


FIG. 10. Dispersion curve for L mode guided by MIR chain based on heavily doped silicon.  $a = 80 \text{ nm}$ ,  $d = 60 \text{ nm}$ , and  $\epsilon_b = 2.25$ . (a) Real part of  $k$ ; (b) Imaginary part of  $k$ . Dashed line in (a) is background light line. Inset shows the permittivity of doped silicon around the guidance frequency range.

background medium has standard  $\epsilon_b = 2.25$ . The imaginary part of the mode's propagation constant (Fig. 10b) is however found to be quite large in general. After conversion, the corresponding propagation length hardly goes beyond 100 nm, with the longest at 96 nm when  $\omega = 0.405\omega_0$ .

#### IV. DISCUSSION AND CONCLUSION

To conclude, a versatile FEM-based mode solver was formulated and used to investigate modal properties of plasmonic chain waveguides in a few varieties. The investigation started from chain waveguides made of non-dispersive negative-epsilon materials. In this way, "waveguide dispersion" of both T and L modes were examined. The T modes can have dispersion curves with a local maximum in the first Brillouin zone; the curve section after the plateau point has negative group velocity and amplifying amplitude when material loss is present. While the T mode tends to exhibit flat band, the L mode is found to be able to span over a large frequency range. Moreover, the L mode can stay far below light line of background medium, which hints the possibility of achieving deep-subwavelength light guidance. Our analyses then moved on to show the performance of chain waveguides made of realistic plasmonic metals in various material and geometrical configurations. The silver chain waveguide, with the geometry and background considered, can be promising for achieving  $1 \mu\text{m}$  light propagation, especially with its T mode. One has to motivate the use of a chain waveguide through some figure of merit based on loss and mode confinement. The L mode achieves  $> 1 \mu\text{m}$  propagation length (but not

over  $2\ \mu\text{m}$ ) in a very narrow frequency range. At MIR wavelength, as a demonstration, we numerically showed that a chain waveguide with plasmonic particles being doped silicon can achieve deep-subwavelength light guidance, which can be useful for sensing and thermal applications. The advantage of the so-called hetero-plasmonic chain waveguide can be doubtful. Effectively it can be treated as a superposition of two chain waveguides. Inclusion of silver particles reduces the loss of a gold chain waveguide; but the silver waveguide can be adversely affected by presence of gold particles. A chain waveguide sitting on a dielectric substrate was also examined. There we noticed degeneracy breakup of T-mode pair, and dominant presence of L mode.

In general, with realistic plasmonic materials, *sub-wavelength* chain modes have very limited propagation lengths. The best material among those we investigated is, unsurprisingly, silver. But still, its subwavelength modes have propagation lengths comparable to the input light wavelength in free space. Despite heavy losses, chain waveguides offers more degrees of freedom

in engineering modal properties. Although we have not attempted in this work, there should be room for improvements through geometrical optimization. Its deep-subwavelength mode confinement, locally enhanced field intensity, as well as its unusual polarization could be useful for special nanophotonic applications including sensing and nonlinear optics.

## ACKNOWLEDGEMENT

The Swedish Research Council (Ventenskapsrådet, or VR), through project no. 2016-03911 as well as its Linnaeus center in Advanced Optics and Photonics (ADOPT), is deeply acknowledged. The FEM computations were performed on resources provided by the Swedish National Infrastructure for Computing (SNIC) at PDC - Center for High Performance Computing at KTH. S. Macinkevicius is thanked for cheerful discussion on semiconductors.

- 
- [1] M. Quinten, A. Leitner, J. R. Krenn, and F. R. Aussenegg, *Opt. Lett.* **23**, 1331 (1998).
- [2] S. Fan, J. D. Joannopoulos, J. N. Winn, A. Devenyi, J. C. Chen, and R. D. Meade, *Journal of the Optical Society of America B* **12**, 1267 (1995)
- [3] A. Yariv, Y. Xu, R. K. Lee, and A. Scherer, *Opt. Lett.* **24**, 711 (1999).
- [4] P. Cheben, D.-X. Xu, S. Janz, and A. Densmore, *Opt. Express* **14**, 4695 (2006).
- [5] W. H. Weber and G. W. Ford, *Physical Review B - Condensed Matter and Materials Physics* **70**, 041401 (2004)
- [6] K. H. Fung and C. T. Chan, *Optics Letters* **32**, 973 (2007), arXiv:0610269 [physics].
- [7] M. Conforti and M. Guasoni, *Journal of the Optical Society of America B* **27**, 1576 (2010).
- [8] M. Guasoni and M. Conforti, *Journal of the Optical Society of America B* **28**, 1019 (2011).
- [9] J.-W. Dong and Z.-L. Deng, *Optics letters* **38**, 2244 (2013).
- [10] P. J. Compaijen, V. A. Malyshev, and J. Knoester, *Optics Express* **23**, 2280 (2015).
- [11] K. B. Crozier, E. Togan, E. Simsek, and T. Yang, *Opt. Express* **15**, 17482 (2007).
- [12] J. Krenn, A. Dereux, J. Weeber, E. Bourillot, Y. Lacroute, J. Goudonnet, G. Schider, W. Gotschy, a. Leitner, F. Aussenegg, and C. Girard, *Physical Review Letters* **82**, 2590 (1999).
- [13] E.-M. Roller, L. V. Besteiro, C. Pupp, L. K. Khorashad, A. O. Govorov, and T. Liedl, *Nature Physics* **13**, 761 (2017).
- [14] R. Soref, R. E. Peale, and W. Buchwald, *Opt. Express* **16**, 6507 (2008).
- [15] J. C. Ginn, R. L. Jarecki, E. A. Shaner, and P. S. Davids, *Journal of Applied Physics* **110**, 043110 (2011).
- [16] N. J. Kramer, K. S. Schramke, and U. R. Kortshagen, *Nano Letters* **15**, 5597 (2015), pMID: 26214245.
- [17] H. Zhang, R. Zhang, K. S. Schramke, N. M. Bedford, K. Hunter, U. R. Kortshagen, and P. Nordlander, *ACS Photonics* **4**, 963 (2017).
- [18] M. Davanco, Y. Urzhumov, and G. Shvets, *Opt. Express* **15**, 9681 (2007).
- [19] G. Parisi, P. Zilio, and F. Romanato, *Opt. Express* **20**, 16690 (2012).
- [20] P. Cheben, R. Halir, J. H. Schmid, H. A. Atwater, and D. R. Smith, *Nature* **560**, 565 (2018).
- [21] P. B. Johnson and R. W. Christy, *Phys. Rev. B* **6**, 4370 (1972).
- [22] M. Yan, *Journal of Optics* **15**, 025006 (2013).
- [23] In fact, many modal dispersion calculations in the current work started with reduced or totally suppressed material losses. Such practice facilitates quick location of the bands.
- [24] J. Wang, Y. Chen, X. Chen, J. Hao, M. Yan, and M. Qiu, *Optics Express* **19**, 14726 (2011).
- [25] X. Chen, Y. Chen, M. Yan, and M. Qiu, *ACS Nano* **6**, 2550 (2012), pMID: 22356648.
- [26] X. Chen, Y. Chen, J. Dai, M. Yan, D. Zhao, Q. Li, and M. Qiu, *Nanoscale* **6**, 1756 (2014).
- [27] C. Jacoboni, C. Canali, G. Ottaviani, and A. A. Quaranta, *Solid-State Electronics* **20**, 77 (1977).